Revision 1

Understanding the unique geochemical behavior of Sc in the interaction with clay minerals

YINGCHUN ZHANG,[†, ‡] XIANDONG LIU,[*, †, ‡] XIANCAI LU,[†, ‡] RUCHENG WANG[†, ‡]

[†]State Key Laboratory for Mineral Deposits Research, School of Earth Sciences and Engineering, Nanjing University, Nanjing, Jiangsu 210023, P. R. China

[‡]Frontiers Science Center for Critical Earth Material Cycling, Nanjing University, Nanjing, Jiangsu 210023, P. R. China

* Corresponding author: xiandongliu@nju.edu.cn. Tel: +86 25 83594664, Fax: +86 25 83686016.

ABSTRACT

Regolith-hosted rare earth elements (REEs) deposits received great attention due to the increasing incorporation of REEs in modern technologies. In lateritic Sc deposits and ion-adsorption deposits (IADs), Sc behaves quite differently from other REEs: REEs adsorb as outer-sphere complexes on clay surface in IADs while Sc could enter the lattice of clay minerals in lateritic Sc deposits. The unique behavior of Sc has not been well understood yet. Here, by using first-principles molecular dynamics techniques, we show that the complexation mechanisms of Y^{3+} and Sc^{3+} on clay edge surfaces are distinctly different. Y^{3+} preferentially adsorbs on $Al(OH)_2SiO$ site with its coordination water protonated. Sc^{3+} is found to behave similarly to other first-row transition metals (e.g. Ni^{2+}) due to its smaller ionic radius and prefers adsorbing on the vacancy site, from where Sc^{3+} can be readily incorporated in the clay lattice. The H_2O ligands of Sc^{3+} get deprotonated upon complexation, providing new binding sites for further enrichment of Sc^{3+}. These processes prevent Sc^{3+} from being leached during weathering and lead to the formation of Sc-rich clay minerals found in lateritic deposits. Based on these results, it is revealed that the small ionic radius and high affinity to enter the vacancy on edge surfaces make Sc compatible with clay minerals and are the origin of its unique geochemical behavior.

Keywords: Scandium, rare earth elements, clay minerals, complexation mechanisms, first principles molecular dynamics

INTRODUCTION

Rare earth elements (REEs, i.e. scandium, yttrium, and 15 lanthanoids) are finding increasing use in modern high-tech industries such as electronics manufacture, green energy technologies, and military applications (Chakhmouradian and Wall, 2012; Williams-Jones and Vasyukova, 2018) and they have been classified as strategic and critical elements worldwide (Haxel, 2002; Gulley et al., 2018; Zhai et al., 2019). Among different REEs deposits, regolith-hosted deposits have received significant attention due to the enrichment and ease of extraction of high-value elements (Zhou et al., 2020). Ion-adsorption deposits (IADs) developed in South China are currently the dominant sources for heavy REEs (Hoshino et al., 2016) while the lateritic deposits recently found in Australia are regarded as a potential long-term Sc resources (Jaireth et al., 2014; Chassé et al., 2016; Chassé et al., 2019). Clay minerals played a pivotal role during the formation of these deposits (Li et al., 2017; Chassé et al., 2019; Borst et al., 2020; Elliott, 2020; Li and Zhou, 2020). In IADs, REEs were believed to be weakly adsorbed on clay minerals (i.e. in outer-sphere complexes) due to their easy-extraction nature (Bao and Zhao, 2008; Borst et al., 2020). In lateritic Sc deposits, however, Sc was found to be incorporated in the lattice of clay minerals before its association with goethite (Chassé et al., 2019).

The unique behavior of Sc compared with other REEs regarding the interaction with clay minerals is still poorly understood. Sc and other REEs exhibit very high hydration

54 enthalpy (Rizkalla and Choppin, 1991; Cotton, 2013) and therefore, they all form out-
55 er-sphere complexes on clay basal surfaces. Thus, it can be deduced that the uniqueness
56 of Sc originates from its interaction with clay edge surface. However, the role clay edges
57 played in the partition of REEs remains unclear. Recently, Borst et al. (2020) presented
58 X-ray absorption fine structure (EXAFS) evidence confirming that outer-sphere com-
59 plexes on basal surface are the dominant forms of REEs in IAD. The existence of in-
60 ner-sphere complexes on clay edges, however, cannot be excluded by the authors, espe-
61 cially when the pH increment with depth was considered (Li et al., 2019; Li et al., 2020;
62 Huang et al., 2021). Indeed, there are a number of experimental studies that support the
63 existence of inner sphere complexes on clay edges in mildly acidic to basic conditions
64 (Stumpf et al., 2002; Kowal-Fouchard et al., 2004; Takahashi et al., 2004; Verma et al.,
65 2014; Zhou et al., 2021; Zhou et al., 2022). Using polarized EXAFS technique, Schlegel
66 and Finck et al. investigated the complexation of Y^{3+} and Lu^{3+} on hectorites and suggest-
67 ed the existence of inner-sphere complexes on the edge surfaces that coordinated to both
68 octahedral and tetrahedral sheets (Schlegel, 2008; Finck et al., 2009; Finck et al., 2017).
69 The structures of such inner-sphere complexes, however, were not unambiguously deter-
70 mined. For example, both six- and eight-fold coordinations have been suggested for Y^{3+}
71 (Schlegel, 2008; Finck et al., 2017). The complexation mechanism of Sc^{3+} on clay edge
72 surfaces has not been studied to the best of our knowledge. Similar to Sc^{3+}, Ni^{2+} could be
73 enriched in phyllosilicates in lateritic deposits, where Ni^{2+} is incorporated in the lattice of

clay minerals (Butt and Cluzel, 2013). It was found that clay edge surfaces acted as both complexation and nucleation sites for the formation of Ni-bearing clay minerals in lateritic Ni deposits (Dähn et al., 2002; Dähn et al., 2003; Zhang et al., 2019b; Liu et al., 2022).

Here, we demonstrate that the unique behavior of Sc originates from its high affinity to enter the vacancy on clay edges using *ab initio* molecular dynamics (AIMD) technique. AIMD method has proven to be powerful in quantifying the structural and thermodynamical properties of mineral-cation interactions (Alexandrov and Rosso, 2015; Kubicki, 2016; Leung et al., 2018; Liu et al., 2022). We determined the complexation structures and the associated free energy changes of Sc^{3+} on montmorillonite (010) edge and made comparison with Y^{3+}.Y^{3+} is enriched in IADs in South China (Zhou et al., 2020) and here it is selected as an example of heavy REEs. The complexation free energies of Sc^{3+} and Y^{3+} on (010) surface were calculated using the method of constraint. The acidity constants of their surface complexes were calculated using AIMD based vertical energy gap method to determine their protonation states in common pH conditions. The results suggest that Y^{3+} would preferentially adsorb on the $Al(OH)_2SiO$ site in a pentagonal bipyramid geometry with its coordination water protonated. In contrast, Sc^{3+} is embedded into the vacancy with all the coordination water deprotonated and the complexation free energy is significantly higher than its complex on the $Al(OH)_2$ site. Complexation of Y^{3+} prohibits its further adsorption on the edge surface while Sc^{3+} complexed provides addi-

tional binding sites for further complexation. This process contributes to the enrichment of Sc and leads to the formation of Sc-rich clay minerals found in the lateritic Sc deposits. The findings presented in this study provides an atomic level insight into the unique geochemistry of Sc^{3+} and forms a microscopic basis for development of efficient REEs extraction techniques.

COMPUTATIONAL METHODS

Atomistic model

The clay (010) and (110) edge surface models were taken from previous studies (Zhang et al., 2020) and contained 3 × 1 × 1 unit cells. 15 water molecules were placed in the interlayer region to represent the monolayer hydrate state, corresponding to a basal spacing of 12.5 Å. One isomorphic substitution of Mg for Al was imposed and one Li^+ was used as the counterion in the interlayer region. The surface model was placed in 3D periodically repeated orthorhombic box and surmounted by a ~15 Å thick solution region that contains 86 water molecules. The dimensions of the simulation box were 25 Å × 15.54 Å × 12.5 Å.

AIMD simulations

All AIMD simulations were carried out using the CP2K/QUICKSTEP package (VandeVondele et al., 2005; Kühne et al., 2020) where the electronic structures were calculated with density functional theory (DFT). With the dual-basis set Gaussian and plane wave (GPW) scheme (Lippert et al., 1997), the electronic wavefunctions were construct-

ed using a double-ζ Gaussian-type orbital basis (VandeVondele and Hutter, 2007) with polarization functions (DZVP) and the electron density was represented with the plane-wave basis expanded to 360 Ry. The core electron states were described using Goedecker-Teter-Hutter (GTH) pseudopotentials (Goedecker et al., 1996). The exchange-correlation was accounted for with Perdew–Burke–Ernzerhof (PBE) functional (Perdew et al., 1997). The DFT-D3 functional was adopted for van der Waals corrections (Grimme et al., 2010). Wave functions were optimized to a tolerance of 1.0E-6.

Born-Oppenheimer type molecular dynamics (BOMD) simulations were carried out in NVT ensemble with temperature controlled at 300 K using a Nosé-Hoover chain thermostat. For each simulation, a production run was performed for over 15.0 ps after an equilibration run for at least 5.0 ps.

Constrained AIMD

The complexation free energy was calculated with constrained AIMD (Sprik and Ciccotti, 1998). In this method, the free energy profile was obtained by integrating the mean forces along a specified reaction coordinate. In this study, the distance from Sc^{3+}/Y^{3+} to the plane defined by three surface oxygen atoms (i.e., two O in AlOH and one O in SiO(H)) was selected as the reaction coordinate. A similar reaction coordinate has been shown to be able to describe the desorption processes of REEs from mineral surface (Leung et al., 2021). The outer-sphere form was taken as the final state of the desorption process.

pKa calculations

The intrinsic pKas of Sc^{3+}/Y^{3+} surface complexes were evaluated with the half-reaction scheme of the vertical energy gap method (Sulpizi and Sprik, 2008; Cheng et al., 2009; Costanzo et al., 2011; Cheng and Sprik, 2012). The deprotonation free energy was calculated as the integral of the ensemble averages of the vertical energy gaps along the alchemical path from reactant state to product state. We refer the readers to our previous papers for the details (Cheng et al., 2014).

RESULTS AND DISCUSSION

Complex structures

There are several sites possible for complexing transition metal cations (e.g. Cd^{2+} and Ni^{2+}) on clay edge surfaces, including the SiO site, the $Al(OH)_2$ site, and the vacancy site, with the latter two being more favorable (Alexandrov and Rosso, 2013; Zhang et al., 2017). Possible Sc^{3+}/Y^{3+} complexes on (010) surface were firstly probed with free AIMD simulations. Y^{3+} and Sc^{3+} were initially placed on the $Al(OH)_2$ and vacancy sites (Fig. 1a). During the simulation, Y^{3+} initially complexed on the vacancy site gradually transferred to the $Al(OH)_2SiO$ site (Fig. 1b). This complexation site has not been reported for other transition metals like Ni^{2+} and Cd^{2+} (Zhang et al., 2016; Zhang et al., 2017), which could be explained by the larger ionic radius of Y^{3+}. The average Y^{3+}-O distance on this site was 2.36 Å. On this site, Y^{3+} was seven-fold coordinated (i.e., four H_2O ligands, two

AlOHs, and one SiO) in a slightly irregular pentagonal bipyramid cage. Y^{3+} located slightly above the octahedral plane on this site, similar to the structure suggested by Schlegel (2008). On $Al(OH)_2$ site, Y^{3+} was eight-fold coordinated with six H_2Os and two AlOHs in a square antiprism geometry (Fig. 1c), where Y^{3+} resided on the octahedral plane. Such a coordination environment could minimize the inter-ligand repulsions (Thompson, 1979) and resembles the structure predicted for the Y^{3+} aqua ion (Díaz-Moreno et al., 2000; Liu et al., 2012). The average Y^{3+}-O distance was 2.41 Å, which was in good agreement with the values reported for the eight-fold coordinated Y^{3+} in previous studies (i.e., 2.35 Å~2.46 Å) (Matsubara et al., 1990; Díaz-Moreno et al., 2000; Ikeda et al., 2004; Liu et al., 2012).

Sc^{3+} was six-fold coordinated with four H_2Os and two AlOHs on the $Al(OH)_2$ site (Fig. 1d). Sc^{3+} exhibited a regular octahedron coordination geometry and located at the mid-plane of the clay TOT sheet. The average Sc^{3+}-O distance was 2.13 Å. On the vacancy site, the two water ligands of Sc^{3+} dissociated spontaneously during the simulation and thus the resulting stable structure was a slightly irregular octahedron where Sc^{3+} was six-coordinated with four surface O atoms and two OHs (Fig. 1e). The average distances between Sc^{3+} and apical O, O atoms of AlOH, and OH were 2.48 Å, 2.10 Å, and 1.99 Å, respectively. The spontaneous dissociation of the coordination water was consistent with its strong acidic nature as demonstrated in the following section.

The complexation structures of Sc^{3+} and Y^{3+} show that these two cations share a

same complexing site, i.e. the $Al(OH)_2$ site. Apart from this site, they also have different complexing sites, that is, vacancy site for Sc^{3+} and $Al(OH)_2SiO$ site for Y^{3+}. The complexation structures on these two sites are compared in Fig. 2. It can be seen that while Y^{3+} is clearly off the edge plane, Sc^{3+} resembles the lattice Al position, that is, Sc^{3+} is embedded into the octahedral sheet (Fig. 2). In our previous study, we derived the complexation structures of transition metals on the vacancy site and found that cations including Ni^{2+}, Co^{2+}, Fe^{2+} and Cu^{2+} fit well in the vacancy while Cd^{2+} is clearly off the vacancy center (Zhang et al., 2017; Zhang et al., 2019a). Based on these observations, it was proposed that cations smaller than Cd^{2+} (e.g. Ni^{2+}) could enter the clay lattice. The complexation structure of Sc^{3+} in Fig. 2 suggests that this rule also applies for Sc^{3+}: Sc^{3+} is indeed smaller than Cd^{2+} (i.e. 0.83 Å *V.S.* 1.03 Å) (Whittaker and Muntus, 1970). This indicates that Sc^{3+} behaves similarly to first-row transition metals in interaction with clay minerals.

Besides (010) surface, (110) surface is also a major edge surface of clay minerals. Additional AIMD simulations show that the complexation structures of Sc^{3+} and Y^{3+} on (110) surface are similar to their counterparts on (010) surface (Online Material[1] Fig. OM1). Y^{3+} formed a pentagonal bipyramid complex bonded to both the octahedral sheet and tetrahedral sheet on the $(AlOH)_2SiO$ site and a square antiprism complex on the (AlOH)(AlSiO) site on (110) surface (Online Material[1] Fig. OM1). Sc^{3+} formed octahedral complexes on both the (AlOH)(AlSiO) site and the vacancy site on (110) surface. On

194 the vacancy site, one H_2O ligand of Sc^{3+} dissociated spontaneously during the AIMD
195 simulation. Similar to the cases on (010) surface, Y^{3+} complexes on (110) surface are
196 clearly off the edge plane while Sc^{3+} fits well in the octahedral vacancy on (110) surface
197 and is embedded into the clay octahedral sheet.

198 The complexation structure of Lu^{3+} (i.e. the smallest lanthanide) on the vacancy site
199 was also obtained from AIMD simulation. The complexation structure (Fig. 2c) clearly
200 shows that Lu^{3+} formed a bidentate complex on the vacancy site and was away from the
201 edge plane. Therefore similar to Y^{3+}, Lu^{3+} cannot enter the vacancy.

202 Based on the above structures, the stable surface complexes for Y^{3+} and Sc^{3+} on (010)
203 surface are determined to be: seven-fold coordinated pentagonal bipyramid for Y^{3+} on
204 $Al(OH)_2SiO$ site, eight-fold coordinated square antiprism for Y^{3+} on $Al(OH)_2$ site, and
205 six-fold coordinated octahedra for Sc^{3+} on $Al(OH)_2$ and vacancy sites. To better under-
206 stand the complexation mechanisms of Y^{3+} and Sc^{3+}, these structures were used as the
207 initial configurations in the following sections to calculate the complexation free energies
208 and pKas of these complexes.

209

210 **Complexation free energies**

211 The stabilities of the four surface complexes were probed by calculating the free en-
212 ergy changes from the inner-sphere states to the outer-sphere states. The free energies
213 were obtained by using the constrained AIMD method and the distances between

This is the peer-reviewed, final accepted version for American Mineralogist, published by the Mineralogical Society of America.
The published version is subject to change. Cite as Authors (Year) Title. American Mineralogist, in press.
DOI: https://doi.org/10.2138/am-2023-8941. http://www.minsocam.org/

Y^{3+}/Sc^{3+} and the edge surface plane were selected as the reaction coordinate. The first and second pKas of Sc^{3+} aqua ion are 4.3 and 5.4 respectively (Baes and Mesmer, 1976), indicating that Sc^{3+} is doubly deprotonated in near neutral pH environment. In contrast, the first pKa of Y^{3+} aqua ion is 7.7 (Baes and Mesmer, 1976), that is, the H_2O ligands of Y^{3+} hardly deprotonate in mildly acidic pH. Therefore, Y^{3+} and $Sc(OH)_2^+$ were used in the free energy calculations. The obtained free energy curves and representative intermediate structures are shown in Fig. 3.

On the $Al(OH)_2$ site, Y^{3+} was bidentately coordinated and formed a square antiprism coordination at d = 1.95 Å (Fig. 3). As Y^{3+} left the surface, the free energy curve gradually went up (Fig. 3a). At d = 2.8 Å, one Y^{3+}-OH bond broke and Y^{3+} transformed into a monodentate complex in mono-capped trigonal prismatic geometry (Fig. 3c). As the distance increased to 3.1 Å, one solvent water molecule entered the hydration shell of Y^{3+} and the free energy curve started to decrease. At d = 3.6 Å, Y^{3+} transformed to an outer-sphere complex in pentagonal bipyramid coordination. The free energy curve reached the local minima at this distance and the corresponding free energy change was 22.4 kcal/mol, indicating that Y^{3+} complexed on the $Al(OH)_2$ site is fairly stable.

On the $Al(OH)_2SiO$ site, the desorption of Y^{3+} included three successive bond breaking events (Fig. 3c), that is, the breakage of the two Y^{3+}-AlOH bonds and the Y^{3+}-SiO bond (at d = 1.8 Å, 2.2 Å and 2.8 Å respectively). At the initial state (i.e., d = 1.4 Å), Y^{3+} formed a tridentate complex in pentagonal bipyramid geometry. As the distance

234 increased to 1.8 Å, one Y^{3+}-AlOH bond broke and the coordination shell of Y^{3+} trans-
235 formed into an octahedron. With the further increasing of the distance, two solvent water
236 molecules entered the hydration shell of Y^{3+} successively at 2.2 Å and 2.4 Å and Y^{3+}
237 changed into the pentagonal bipyramid coordination. At d = 2.8 Å, Y^{3+} coordinated with
238 another solvent water molecule and the Y^{3+}-SiO bond broke. The free energy curve start-
239 ed to decrease at this distance and reached the local minima at d = 3.4 Å, where Y^{3+}
240 formed an outer-sphere complex in a mono-capped trigonal prism. The free energy
241 change for the desorption process of Y^{3+} from $Al(OH)_2SiO$ site was calculated to be 29.8
242 kcal/mol. This value suggests that Y^{3+} complexed on the $Al(OH)_2SiO$ site is substantially
243 more stable than that on the $Al(OH)_2$ site and Y^{3+} would preferentially adsorb on the
244 $Al(OH)_2SiO$ site. Y^{3+} is bonded to one SiO group and two AlOH groups on the
245 $Al(OH)_2SiO$ site. The AlOH groups also belong to the $Al(OH)_2$ site and the complex on
246 $Al(OH)_2SiO$ occupies the binding sites of $Al(OH)_2$. Therefore, complexation on the
247 $Al(OH)_2$ site actually hardly happen due to the strong steric repulsions imposed by Y^{3+}
248 complex on the $Al(OH)_2SiO$ site. This is in agreement with the previous EXAFS meas-
249 urement which suggested Y^{3+} was tilted away from the mid-plane of the clay TOT sheet
250 (Schlegel, 2008).

251 $Sc(OH)_2^+$ formed a stable bidentate complex on the $Al(OH)_2$ site with a distance of
252 1.8 Å from the surface (Fig. 3d). This distance is shorter than the value obtained for Y^{3+}
253 (i.e., 1.80 Å *V.S.* 1.95 Å), in agreement with its smaller ionic radius (0.83 Å *V.S.* 1.10 Å)

(Whittaker and Muntus, 1970). During the desorption process, the two Sc^{3+}-AlOH bonds dissociated successively at d = 2.4 Å and 2.9 Å respectively. The coordination shell of Sc^{3+} was compensated by two solvent water molecules after Sc^{3+}-AlOH dissociations and Sc^{3+} kept the octahedral geometry during the entire desorption process. The local minima on the free energy curve located at d = 3.6 Å, where $Sc(OH)_2^+$ formed a stable outer-sphere complex (Fig. 3b). The free energy required for $Sc(OH)_2^+$ to reach this state was 14.8 kcal/mol.

The detachment of $Sc(OH)_2^+$ from the vacancy site was more complicated than that on the $Al(OH)_2$ site. At the distance of 0.7 Å from the surface plane, Sc^{3+} was incorporated in the octahedral sheet and located near the center of the vacancy (Fig. 3d). As $Sc(OH)_2^+$ left the surface, the bonds between Sc^{3+} and the two apical O atoms gradually broke. At d = 1.4 Å, $Sc(OH)_2^+$ coordinated with one SiOH group and located slightly off the octahedral plane. One solvent water molecule entered the coordination shell of Sc^{3+} at this distance and Sc^{3+} kept its octahedral coordination geometry. As the distance further increased to 2.0 Å, $Sc(OH)_2^+$ transferred onto the $Al(OH)_2$ site spontaneously and captured another water molecule (Fig. 3d). Therefore, the desorption process of $Sc(OH)_2^+$ from the vacancy site can be regarded as a combination of two sub-steps, that is, transfer of $Sc(OH)_2^+$ from the vacancy site to the $Al(OH)_2$ site and the desorption of $Sc(OH)_2^+$ from the $Al(OH)_2$ site. Therefore, the corresponding free energy data after d = 2.0 Å was taken from that of $Sc(OH)_2^+$ on the $Al(OH)_2$ site. The free energy change for the detach-

ment of $Sc(OH)_2^+$ from the vacancy site was 32.4 kcal/mol (Fig. 3b), which was significantly higher than the value obtained for $Sc(OH)_2^+$ on the $Al(OH)_2$ site, implying that $Sc(OH)_2^+$ would adsorb preferentially on the vacancy site. Similarly, the free energy required for Ni^{2+} desorption from the vacancy site was determined to be 58.3 kcal/mol in the previous study, which was significantly higher than the value on the $Al(OH)_2$ site (31.5 kcal/mol) (Zhang et al., 2017).

Hydrolysis of surface complexes

The first and the second pKas of Y^{3+}/Sc^{3+} complexes on different sites calculated using the vertical energy gap method were collected in Table 1. We found that Sc^{3+} complexed on the vacancy site is the most acidic, with the first and second pKas of -6.5 and -0.2 respectively. Such low pKas were consistent with the spontaneous dissociations of water ligands mentioned above. These values were clearly separated from the pKas obtained for other Sc^{3+} and Y^{3+} complexes, i.e. 7.2~8.4. The moderate pKa values for Sc^{3+} complex on $Al(OH)_2$ site, Y^{3+} complexes on $Al(OH)_2$ and $Al(OH)_2SiO$ sites indicate that these complexes could hydrolyze in neutral and basic environments and therefore, both the protonated and deprotonated forms could exist in common pH range. In contrast, for Sc^{3+} complexed on the vacancy site, only the doubly deprotonated form is possible due to the very low pKas.

The first pKas of Sc^{3+} and Y^{3+} aqua ions were measured to be 4.3 and 7.7, respectively (Baes and Mesmer, 1976). Based on the calculated pKas, it can be found that com-

plexation on the vacancy site significantly decreased the pKa of Sc^{3+}. Such a decrease was also found in our prior study for Ni^{2+} complexed on this site (i.e. 8.4 *V.S.* 10.4) (Zhang et al., 2017). For Y^{3+}, however, complexation on clay edge had little influence on its pKa (i.e. 7.2~8.2 *V.S.* 7.7).

IMPLICATIONS

According to the structures, free energies, and the pKas of surface complexes, an atomic level understanding of the complexation mechanisms of Sc^{3+} and Y^{3+} can be obtained. Y^{3+} prefers adsorbing on the $Al(OH)_2SiO$ site as a pentagonal bipyramid complex. Complexation on this site prohibits the complexation of Y^{3+} on the $Al(OH)_2$ site due to the consumption of the AlOH binding sites. The H_2O ligands of Y^{3+} keeps protonated upon complexation, especially in the acidic to slightly basic environment found in IADs.

Sc^{3+} behaves differently from Y^{3+} in that it preferentially adsorbs on the vacancy site and forms an octahedral complex that fits well in the vacancy. The free energy required to desorb Sc^{3+} from this site is obviously higher than that on the $Al(OH)_2$ site, suggesting that detachment of Sc^{3+} from clay edge surfaces hardly occur. Different from Y^{3+}, complexation of Sc^{3+} on the vacancy site significantly reduces the pKas of its H_2O ligands and results in the deprotonation of these ligands. All of the aforementioned characteristics were also observed for Ni^{2+}, which could be readily incorporated in the octahedral sheet (Zhang et al., 2017). Moreover, the pKas of H_2O ligands of Ni^{2+} also decreased upon

complexation on the vacancy site, which makes the deprotonation easier (Zhang et al., 2017). The OH groups formed after the deprotonation of H_2O ligands were found to be able to complex additional Ni^{2+}, leading to the formation of multinuclear complexes and even the nucleation of hydroxide or phyllosilicates (Zhang et al., 2019a; Zhang et al., 2019b). Thus, one can expect that similar processes also happen to Sc^{3+}, that is, Sc^{3+} could form multinuclear complexes on clay edge surfaces. During the supergene weathering of Sc-bearing silicates (e.g. amphibole and clinopyroxene (Chassé et al., 2019)), the thus-formed multinuclear complexes can be readily silicificated due to the abundance of Si in fluids.

During the formation of lateritic Sc deposits, Sc^{3+} was found to be enriched in the clay phase (up to hundreds of ppm) (Chassé et al., 2019). The findings presented here provide an atomic level clue for understanding the formation of the Sc-rich clays: during the weathering process, Sc^{3+} released from parent rocks preferentially adsorbs on the vacancy site on clay edges; the H_2O ligands of Sc^{3+} readily get deprotonated upon complexation, providing new binding sites for complexation of additional Sc^{3+}; this process leads to the nucleation and growth of Sc-rich clays, which can effectively prevent Sc from being leached.

Overall, the results obtained in the present study suggest that Y^{3+} and Sc^{3+} have distinctly different complexation mechanisms on clay edge surfaces. This difference arises from the smaller ionic radius of Sc^{3+} and its high affinity to the vacancy on clay edge,

334 which makes Sc compatible with clay minerals and behave similarly to some transition
335 metals (e.g. Ni^{2+}) at the atomic level (i.e. complexation sites, relative stabilities, and hy-
336 drolysis). These effects together contribute to the unique geochemical behavior of Sc ob-
337 served in the deposits.
338
339

ACKNOWLEDGMENTS AND FUNDING

This study was supported by the National Natural Science Foundation of China (No. 42125202) and China Postdoctoral Science Foundation (No. 2022M721547). We acknowledge the financial support from the State Key Laboratory for Mineral Deposits Research at Nanjing University. We are grateful to the High Performance Computing Center (HPCC) of Nanjing University for doing the numerical calculations in this paper on its blade cluster system.

REFERENCES CITED

Alexandrov, V., and Rosso, K.M. (2013) Insights into the Mechanism of Fe(II) Adsorption and Oxidation at Fe–Clay Mineral Surfaces from First-Principles Calculations. The Journal of Physical Chemistry C, 117(44), 22880-22886.

-. (2015) Ab initio modeling of Fe(ii) adsorption and interfacial electron transfer at goethite (α-FeOOH) surfaces. Physical Chemistry Chemical Physics, 17(22), 14518-14531.

Baes, C.F.J., and Mesmer, R.E. (1976) The Hydrolysis of Cations. Wiley-Interscience, New York.

Bao, Z., and Zhao, Z. (2008) Geochemistry of mineralization with exchangeable REY in the weathering crusts of granitic rocks in South China. Ore Geology Reviews, 33(3), 519-535.

Borst, A.M., Smith, M.P., Finch, A.A., Estrade, G., Villanova-de-Benavent, C., Nason, P., Marquis, E., Horsburgh, N.J., Goodenough, K.M., Xu, C., Kynický, J., and Geraki, K. (2020) Adsorption of rare earth elements in regolith-hosted clay deposits. Nature Communications, 11(1), 4386.

Butt, C.R.M., and Cluzel, D. (2013) Nickel Laterite Ore Deposits: Weathered Serpentinites. Elements, 9(2), 123-128.

Chakhmouradian, A.R., and Wall, F. (2012) Rare Earth Elements: Minerals, Mines, Magnets (and More). Elements, 8(5), 333-340.

Chassé, M., Griffin, W.L., O'Reilly, S.Y., and Calas, G. (2016) Scandium Speciation in a World-Class Lateritic Deposit. Geochemical Perspectives Letters, 3(2), 105-114.

Chassé, M., Griffin, W.L., O'Reilly, S.Y., and Calas, G. (2019) Australian laterites reveal mechanisms governing scandium dynamics in the critical zone. Geochimica et Cosmochimica Acta, 260, 292-310.

Cheng, J., Liu, X., VandeVondele, J., Sulpizi, M., and Sprik, M. (2014) Redox Potentials and Acidity Constants from Density Functional Theory Based Molecular Dynamics. Accounts of Chemical Research, 47(12), 3522-3529.

Cheng, J., and Sprik, M. (2012) Alignment of electronic energy levels at electrochemical interfaces. Physical Chemistry Chemical Physics, 14(32), 11245-11267.

Cheng, J., Sulpizi, M., and Sprik, M. (2009) Redox potentials and pK(a) for benzoquinone from density functional theory based molecular dynamics. Journal of Chemical Physics, 131(15), 154504.

Costanzo, F., Sulpizi, M., Valle, R.G.D., and Sprik, M. (2011) The oxidation of tyrosine and tryptophan studied by a molecular dynamics normal hydrogen electrode. The Journal of Chemical Physics, 134(24), 244508.

Cotton, S. (2013) Lanthanide and actinide chemistry. John Wiley & Sons.

Dähn, R., Scheidegger, A.M., Manceau, A., Schlegel, M.L., Baeyens, B., Bradbury, M.H., and Chateigner, D. (2003) Structural evidence for the sorption of Ni(II) atoms on the edges of montmorillonite clay minerals: a polarized X-ray absorption fine

structure study. Geochimica et Cosmochimica Acta, 67(1), 1-15.

Dähn, R., Scheidegger, A.M., Manceau, A., Schlegel, M.L., Baeyens, B., Bradbury, M.H., and Morales, M. (2002) Neoformation of Ni phyllosilicate upon Ni uptake on montmorillonite: A kinetics study by powder and polarized extended X-ray absorption fine structure spectroscopy. Geochimica et Cosmochimica Acta, 66(13), 2335-2347.

Díaz-Moreno, S., Muñoz-Páez, A., and Chaboy, J. (2000) X-ray Absorption Spectroscopy (XAS) Study of the Hydration Structure of Yttrium(III) Cations in Liquid and Glassy States: Eight or Nine-Fold Coordination? Journal of Physical Chemistry A, 104(6), 1278-1286.

Elliott, W.C. (2020) Regolith-hosted rare-earth elements: The phyllosilicate connection. American Mineralogist, 105(1), 1-2.

Finck, N., Bouby, M., Dardenne, K., and Yokosawa, T. (2017) Yttrium co-precipitation with smectite: A polarized XAS and AsFlFFF study. Applied Clay Science, 137, 11-21.

Finck, N., Schlegel, M.L., and Bosbach, D. (2009) Sites of Lu(III) Sorbed to and Coprecipitated with Hectorite. Environmental Science & Technology, 43(23), 8807-8812.

Goedecker, S., Teter, M., and Hutter, J. (1996) Separable dual-space Gaussian pseudopotentials. Physical Review B, 54(3), 1703-1710.

Grimme, S., Antony, J., Ehrlich, S., and Krieg, H. (2010) A consistent and accurate ab initio parametrization of density functional dispersion correction (DFT-D) for the 94 elements H-Pu. Journal of Chemical Physics, 132(15), 154104.

Gulley, A.L., Nassar, N.T., and Xun, S. (2018) China, the United States, and competition for resources that enable emerging technologies. Proceedings of the National Academy of Sciences, 115(16), 4111-4115.

Haxel, G. (2002) Rare earth elements: critical resources for high technology. US Department of the Interior, US Geological Survey.

Hoshino, M., Sanematsu, K., and Watanabe, Y. (2016) Chapter 279 - REE Mineralogy and Resources. In B. Jean-Claude, and P. Vitalij K, Eds. Handbook on the Physics and Chemistry of Rare Earths, 49, p. 129-291. Elsevier.

Huang, J., He, H., Tan, W., Liang, X., Ma, L., Wang, Y., Qin, X., and Zhu, J. (2021) Groundwater controls REE mineralisation in the regolith of South China. Chemical Geology, 577, 120295.

Ikeda, T., Hirata, M., and Kimura, T. (2004) Hydration of Y3+ ion: A Car-Parrinello molecular dynamics study. The Journal of Chemical Physics, 122(2), 024510.

Jaireth, S., Hoatson, D.M., and Miezitis, Y. (2014) Geological setting and resources of the major rare-earth-element deposits in Australia. Ore Geology Reviews, 62, 72-128.

Kowal-Fouchard, A., Drot, R., Simoni, E., Marmier, N., Fromage, F., and Ehrhardt, J.-J. (2004) Structural identification of europium(iii) adsorption complexes on montmorillonite. New Journal of Chemistry, 28(7), 864-869.

Kubicki, J.D. (2016) Molecular modeling of geochemical reactions: an introduction. John Wiley & Sons.

Kühne, T.D., Iannuzzi, M., Del Ben, M., Rybkin, V.V., Seewald, P., Stein, F., Laino, T., Khaliullin, R.Z., Schütt, O., Schiffmann, F., Golze, D., Wilhelm, J., Chulkov, S., Bani-Hashemian, M.H., Weber, V., Borštnik, U., Taillefumier, M., Jakobovits, A.S., Lazzaro, A., Pabst, H., Müller, T., Schade, R., Guidon, M., Andermatt, S., Holmberg, N., Schenter, G.K., Hehn, A., Bussy, A., Belleflamme, F., Tabacchi, G., Glöß, A., Lass, M., Bethune, I., Mundy, C.J., Plessl, C., Watkins, M., VandeVondele, J., Krack, M., and Hutter, J. (2020) CP2K: An electronic structure and molecular dynamics software package - Quickstep: Efficient and accurate electronic structure calculations. The Journal of Chemical Physics, 152(19), 194103.

Leung, K., Criscenti, L.J., Knight, A.W., Ilgen, A.G., Ho, T.A., and Greathouse, J.A. (2018) Concerted Metal Cation Desorption and Proton Transfer on Deprotonated Silica Surfaces. The Journal of Physical Chemistry Letters, 9(18), 5379-5385.

Leung, K., Ilgen, A.G., and Criscenti, L.J. (2021) Interplay of physically different properties leading to challenges in separating lanthanide cations – an ab initio molecular dynamics and experimental study. Physical Chemistry Chemical Physics, 23(10), 5750-5759.

Li, M.Y.H., Zhao, W.W., and Zhou, M.-F. (2017) Nature of parent rocks, mineralization styles and ore genesis of regolith-hosted REE deposits in South China: An integrated genetic model. Journal of Asian Earth Sciences, 148, 65-95.

Li, M.Y.H., and Zhou, M.-F. (2020) The role of clay minerals in formation of the regolith-hosted heavy rare earth element deposits. American Mineralogist, 105(1), 92-108.

Li, M.Y.H., Zhou, M.-F., and Williams-Jones, A.E. (2019) The Genesis of Regolith-Hosted Heavy Rare Earth Element Deposits: Insights from the World-Class Zudong Deposit in Jiangxi Province, South China. Economic Geology, 114(3), 541-568.

-. (2020) Controls on the Dynamics of Rare Earth Elements During Subtropical Hillslope Processes and Formation of Regolith-Hosted Deposits. Economic Geology, 115(5), 1097-1118.

Lippert, B.G., Hutter, J., and Parrinello, M. (1997) A hybrid Gaussian and plane wave density functional scheme. Molecular Physics, 92(92), 477-487.

Liu, X., Lu, X., Wang, R., and Zhou, H. (2012) First-principles molecular dynamics study of stepwise hydrolysis reactions of Y3+ cations. Chemical Geology, 334, 37-43.

Liu, X., Tournassat, C., Grangeon, S., Kalinichev, A.G., Takahashi, Y., and Marques Fernandes, M. (2022) Molecular-level understanding of metal ion retention in clay-rich materials. Nature Reviews Earth & Environment, 3(7), 461-476.

Matsubara, E., Okuda, K., and Waseda, Y. (1990) Anomalous X-ray scattering study of aqueous solutions of YCl3 and ErCl3. Journal of Physics: Condensed Matter,

2(46), 9133-9143.

Perdew, J.P., Burke, K., and Ernzerhof, M. (1997) Generalized Gradient Approximation Made Simple. Physical Review Letters, 78(7), 1396.

Rizkalla, E.N., and Choppin, G.R. (1991) Hydration and hydrolysis of lanthanides. In G.K.A. Jr., and E. L., Eds. Handbook on the Physics and Chemistry of Rare Earths, 15, p. 393-442. Elsevier.

Schlegel, M. (2008) Polarized EXAFS characterization of the sorption mechanism of yttrium on hectorite. Radiochimica Acta, 96(9-11), 667-672.

Sprik, M., and Ciccotti, G. (1998) Free energy from constrained molecular dynamics. The Journal of Chemical Physics, 109(18), 7737-7744.

Stumpf, T., Bauer, A., Coppin, F., Fanghänel, T., and Kim, J.-I. (2002) Inner-sphere, outer-sphere and ternary surface complexes: a TRLFS study of the sorption process of Eu(III) onto smectite and kaolinite. Radiochimica Acta, 90(6), 345-349.

Sulpizi, M., and Sprik, M. (2008) Acidity constants from vertical energy gaps: density functional theory based molecular dynamics implementation. Physical Chemistry Chemical Physics, 10(34), 5238-5249.

Takahashi, Y., Tada, A., and Shimizu, H. (2004) Distribution Pattern of Rare Earth Ions between Water and Montmorillonite and Its Relation to the Sorbed Species of the Ions. Analytical Sciences, 20(9), 1301-1306.

Thompson, L.C. (1979) Chapter 25 Complexes. Handbook on the Physics and Chemistry of Rare Earths, 3, p. 209-297. Elsevier.

VandeVondele, J., and Hutter, J. (2007) Gaussian basis sets for accurate calculations on molecular systems in gas and condensed phases. The Journal of Chemical Physics, 127(11), 114105.

VandeVondele, J., Krack, M., Mohamed, F., Parrinello, M., Chassaing, T., and Hutter, J. (2005) Quickstep: Fast and accurate density functional calculations using a mixed Gaussian and plane waves approach. Computer Physics Communications, 167(2), 103-128.

Verma, P.K., Pathak, P.N., Mohapatra, P.K., Godbole, S.V., Kadam, R.M., Veligzhanin, A.A., Zubavichus, Y.V., and Kalmykov, S.N. (2014) Influences of different environmental parameters on the sorption of trivalent metal ions on bentonite: batch sorption, fluorescence, EXAFS and EPR studies. Environmental Science: Processes & Impacts, 16(4), 904-915.

Whittaker, E.J.W., and Muntus, R. (1970) Ionic radii for use in geochemistry. Geochimica et Cosmochimica Acta, 34(9), 945-956.

Williams-Jones, A.E., and Vasyukova, O.V. (2018) The Economic Geology of Scandium, the Runt of the Rare Earth Element Litter. Economic Geology, 113(4), 973-988.

Zhai, M., Wu, F., Hu, R., Jiang, S., Li, W., Wang, R., Wang, D., Qi, T., Qin, K., and Wen, H. (2019) Critical metal mineral resources: Current research status and scientific issues. Bulletin of National Natural Science Foundation of China, 33(2), 106-111.

Zhang, C., Liu, X., Lu, X., He, M., Jan Meijer, E., and Wang, R. (2017) Surface complexation of heavy metal cations on clay edges: insights from first principles molecular dynamics simulation of Ni(II). Geochimica et Cosmochimica Acta, 203, 54-68.

Zhang, C., Liu, X., Lu, X., Meijer, E.J., Wang, K., He, M., and Wang, R. (2016) Cadmium(II) Complexes Adsorbed on Clay Edge Surfaces: Insight From First Principles Molecular Dynamics Simulation. Clays and Clay Minerals, 64(4), 337-347.

Zhang, C., Liu, X., Lu, X., Meijer, E.J., and Wang, R. (2019a) An atomic-scale understanding of the initial stage of nucleation of heavy metal cations on clay edges. Geochimica et Cosmochimica Acta, 248, 161-171.

-. (2019b) Understanding the Heterogeneous Nucleation of Heavy Metal Phyllosilicates on Clay Edges with First-Principles Molecular Dynamics. Environmental Science & Technology, 53(23), 13704-13712.

Zhang, Y., Liu, X., Zhang, C., and Lu, X. (2020) A combined first principles and classical molecular dynamics study of clay-soil organic matters (SOMs) interactions. Geochimica et Cosmochimica Acta, 291, 110-125.

Zhou, J., Li, M., Yuan, P., Li, Y., Liu, H., Fan, W., Liu, D., and Zhang, H. (2021) Partial rehydration of tubular halloysite (7 Å) immersed in La (NO3) 3 solution for 3 years and its implication for understanding REE occurrence in weathered crust elution-deposited rare earth ores. Applied Clay Science, 213, 106244.

Zhou, J., Liu, H., Liu, D., Yuan, P., Bu, H., Du, P., Fan, W., and Li, M. (2022) Sorption/desorption of Eu(III) on halloysite and kaolinite. Applied Clay Science, 216, 106356.

Zhou, M.F., Li, M.Y.H., Wang, Z.C., Li, X.C., and Liu, J.C. (2020) The genesis of regolith-hosted rare earth element and scandium deposits: Current understanding and outlook to future prospecting. CHINESE SCIENCE BULLETIN-CHINESE, 65(33), 3809-3824.

Endnote:

[1]Online Material.

This is the peer-reviewed, final accepted version for American Mineralogist, published by the Mineralogical Society of America.
The published version is subject to change. Cite as Authors (Year) Title. American Mineralogist, in press.
DOI: https://doi.org/10.2138/am-2023-8941. http://www.minsocam.org/

545 **FIGURE 1**

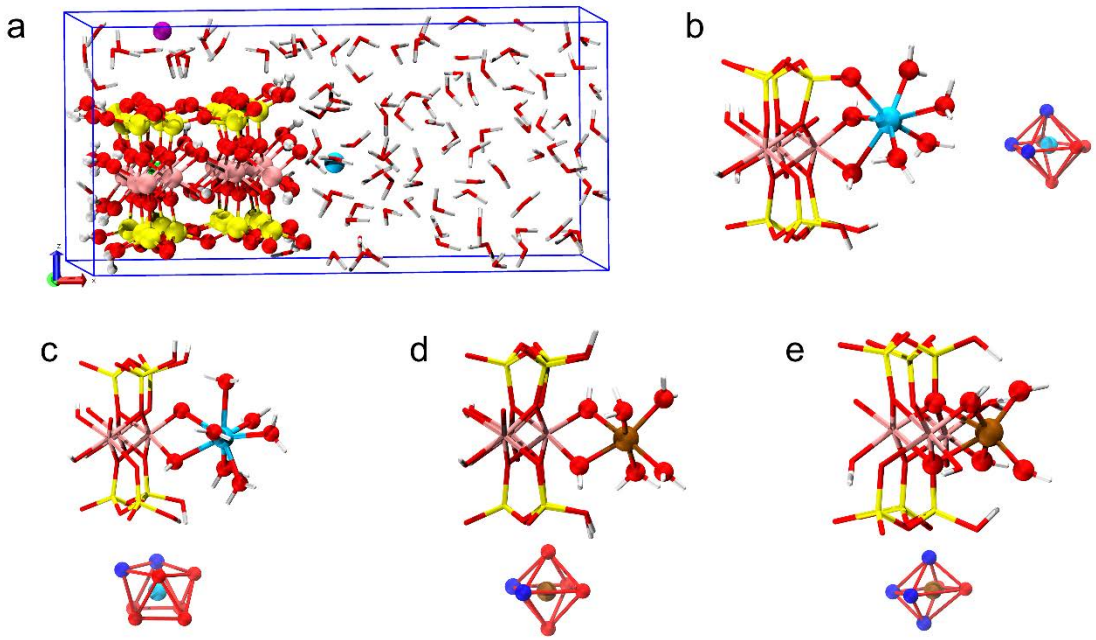

546

547 **FIGURE 1.** Complexation of Sc^{3+}/Y^{3+} on clay (010) surface. **(a)** Simulation box showing
548 the clay surface and solution region. (**b)** and **(c)** Complexation structures of Y^{3+} on the
549 $Al(OH)_2SiO$ site and the $Al(OH)_2$ site, respectively. **(d)** and **(e)** Complexation structures
550 of Sc^{3+} on the $Al(OH)_2$ site and the vacancy site, respectively. O = red, H = white, Si =
551 yellow, Al = pink, Mg = green, Y = cyan, Sc = brown, and Li = purple. Surface O atoms
552 in coordination polyhedra are colored in blue. For clarity, solvent water molecules in
553 **(b)-(e)** are not shown.

554

This is the peer-reviewed, final accepted version for American Mineralogist, published by the Mineralogical Society of America.
The published version is subject to change. Cite as Authors (Year) Title. American Mineralogist, in press.
DOI: https://doi.org/10.2138/am-2023-8941. http://www.minsocam.org/

555 **FIGURE 2**

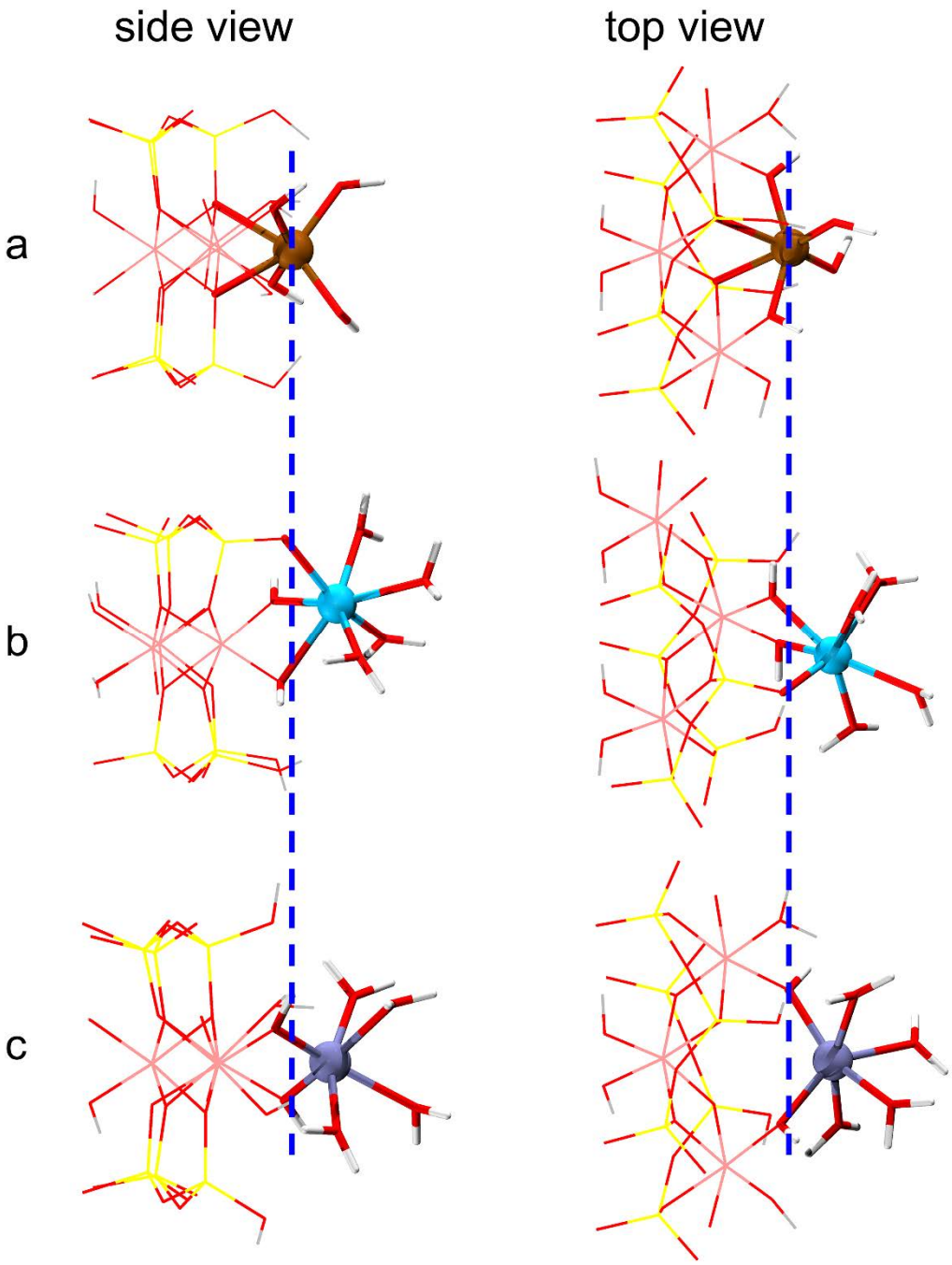

556

557 **FIGURE 2.** Comparison of $Sc^{3+}/Y^{3+}/Lu^{3+}$ complexes on clay (010) surface. **(a)** Sc^{3+}

558 complex on the vacancy site. **(b)** Y^{3+} complex on the $Al(OH)_2SiO$ site. **(c)** Lu^{3+} complex

559 on the vacancy site. Lu is colored in ice-blue and other atoms are color-coded by ele-

This is the peer-reviewed, final accepted version for American Mineralogist, published by the Mineralogical Society of America.
The published version is subject to change. Cite as Authors (Year) Title. American Mineralogist, in press.
DOI: https://doi.org/10.2138/am-2023-8941. http://www.minsocam.org/

560 ments as described in Figure 1. The blue dash lines mark the position of the center of the

561 vacancy.

562

563 **FIGURE 3**

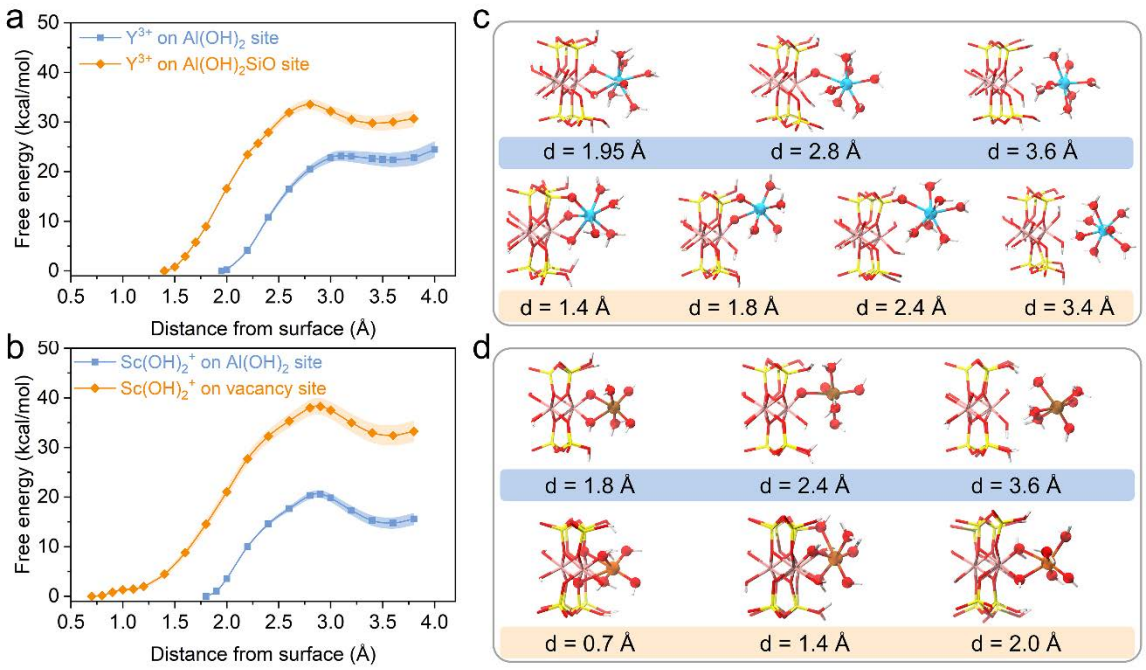

564

565 **FIGURE 3.** Desorption of Y^{3+}/$Sc(OH)_2^+$ from clay edge surface. **(a)** and **(b)** Desorption

566 free energy curves associated with the desorption of Y^{3+} and $Sc(OH)_2^+$. **(c)** and **(d)** Snap-

567 shots showing the complexation structures during the desorption processes. Atoms are

568 color-coded by elements as described in Figure 1.

569

570

571

572 **TABLE 1.** Calculated vertical energy gaps (in eV), thermodynamic integrals (in eV), and

573 pKa values.

Complex	η=0.0	η=0.5	η=1.0	ΔA	p*K*a
$^{Al}Y(H_2O)_5(H_2O)$	20.32±0.01	18.02±0.03	13.65±0.01	17.67±0.02	8.0±0.8
$^{Al}Y(H_2O)_3(OH)(H_2O)$	20.33±0.04	18.15±0.05	13.03±0.02	17.66±0.04	7.8±1.2
$^{Al}H_3O^+$	19.54±0.01	17.34±0.04	13.12±0.04	17.00±0.03	
$^{AlSi}Y(H_2O)_3(H_2O)$	20.12±0.05	18.07±0.04	13.42±0.01	17.64±0.04	8.2±1.0
$^{AlSi}Y(H_2O)_2(OH)(H_2O)$	20.36±0.04	17.85±0.01	13.70±0.03	17.58±0.02	7.2±0.7
$^{AlSi}H_3O^+$	19.66±0.04	17.11±0.01	13.67±0.04	16.96±0.02	
$^{Al}Sc(H_2O)_3(H_2O)$	19.69±0.01	17.76±0.04	14.33±0.05	17.51±0.04	8.4±1.0
$^{Al}Sc(H_2O)_2(OH)(H_2O)$	20.15±0.02	17.95±0.01	13.07±0.04	17.50±0.01	8.2±0.5
$^{Al}H_3O^+$	19.54±0.01	17.06±0.02	13.14±0.04	16.82±0.02	
$^{V}Sc(H_2O)(H_2O)$	19.34±0.05	17.52±0.02	12.89±0.02	17.05±0.03	-6.5±1.0
$^{V}Sc(OH)(H_2O)$	19.77±0.02	17.71±0.04	13.98±0.02	17.43±0.03	-0.2±1.0
$^{V}H_3O^+$	19.57±0.03	17.66±0.03	13.26±0.02	17.25±0.03	

574 The superscript "Al", "AlSi", and "V" stand for complexes on the $Al(OH)_2$ site,

575 $Al(OH)_2SiO$ site, and vacancy site, respectively.

576